Fast computation of analytical second derivatives with effective core potentials: Application to Si 8 C 12 , Ge 8 C 12 , and Sn 8 C 12

Brett M. Bode and Mark S. Gordon

Citation: The Journal of Chemical Physics **111**, 8778 (1999); doi: 10.1063/1.480225
View online: http://dx.doi.org/10.1063/1.480225
View Table of Contents: http://scitation.aip.org/content/aip/journal/jcp/111/19?ver=pdfcov
Published by the AIP Publishing

Fast computation of analytical second derivatives with effective core potentials: Application to Si_8C_{12}, Ge_8C_{12}, and Sn_8C_{12}

Brett M. Bode and Mark S. Gordon
Department of Chemistry, Iowa State University, Ames, Iowa 50011

(Received 3 May 1999; accepted 25 August 1999)

An improved method is described for the computation of integrals involving effective core potentials. The improved method provides better scalability to higher angular momenta as well as improved speed. The new method is also applied to the determination of the minimum energy structures of Si_8C_{12}, Ge_8C_{12}, and Sn_8C_{12}, main group analogs of the Ti_8C_{12} compounds (known as metcars). Relative energies, geometries, and vibrational frequencies are reported for several novel structures. © *1999 American Institute of Physics.* [S0021-9606(99)30243-9]

I. INTRODUCTION

The use of effective core potentials (ECPs)[1] has grown rapidly in recent years as interest in compounds containing elements from the third and subsequent rows of the periodic table has increased. This increase in use has sparked a renewed interest in improving the efficiency of computations involving ECPs. One of the most significant factors influencing the performance of ECPs is the availability of analytic derivatives. Due to the complicated form of the ECP, it is not easy to directly derive analytic derivatives. However, this difficulty was overcome soon after the introduction of the ECP through the application of translational invariance[2,3] to obtain an analytic formula for the energy first derivative (gradient).[4] Later this derivation was extended to include energy second derivatives (Hessians) by Komornicki *et al.*,[5] and has now been implemented by several groups.[6,7] The result of these derivations are the following formulas for the energy, gradient, and Hessian involving ECPs:

$$\text{Energy}\quad E_{\mathrm{ECP}}=\sum_{\mu}\sum_{\nu}\left\langle \phi_{\mu}\left|\sum_{C}\hat{u}_{C}\right|\phi_{\nu}\right\rangle, \tag{1}$$

$$\text{Gradient}\quad E^{a}_{\mathrm{ECP}}=2\sum_{\mu}\sum_{\nu}D_{\mu\nu}\left\langle \phi^{\alpha}_{\mu}\left|\delta_{AI}\sum_{C}\hat{u}_{C}-\hat{u}_{A}\right|\phi_{\nu}\right\rangle, \tag{2}$$

$$\begin{aligned}\text{Hessian}\quad E^{ab}_{\mathrm{ECP}}=2\sum_{\mu}\sum_{\nu}D_{\mu\nu}\Bigg(\Bigg\langle \phi^{\alpha\beta}_{\mu}\Bigg|\sum_{C}\hat{u}_{C}\delta_{AI}\delta_{BI}-\hat{u}_{B}\delta_{AI}\\ -\hat{u}_{A}\delta_{BI}+\hat{u}_{A}\delta_{AB}\Bigg|\phi_{\nu}\Bigg\rangle+\Bigg\langle \phi^{\alpha}_{\mu}\Bigg|\sum_{C}\hat{u}_{C}\delta_{AI}\delta_{BJ}\\ -\hat{u}_{B}\delta_{AI}-\hat{u}_{A}\delta_{BJ}+\hat{u}_{A}\delta_{AB}\Bigg|\phi^{\beta}_{\nu}\Bigg\rangle\Bigg).\end{aligned} \tag{3}$$

E^a refers the derivative of the energy with respect to coordinate a on center A, ϕ_μ and ϕ_ν are basis functions located on centers I and J, respectively; ϕ^{α}_{μ} is the derivative of ϕ_μ with respect to a coordinate of center I,$D_{\mu\nu}$ is an element of the density matrix, $\hat{u}_C$ is the ECP on center C. Since the derivatives of Gaussian type functions are simply linear combinations of Gaussian functions with different angular momenta, these equations all represent the same basic ECP integral. However, a derivative of a Gaussian function raises the maximum angular momentum by one for first derivatives and two for second derivatives. Thus, in order to compute the second derivative of a *g*-type basis function, basic integrals must be computed over *h*- and *i*-type functions. Due to the number of integrals with high angular momenta it is important to compute the ECP integrals efficiently. Since the angular portions of the ECP integrals have simple analytic solutions, the main difficulty in the ECP calculation is the computation of the radial integrals.

II. RADIAL INTEGRAL EVALUATION

There are currently two methods in use for the computation of the radial integrals. The first is the original implementation by Kahn as described in Ref. 1. The second method was proposed by McMurchie and Davidson[8] and has since been improved by several groups.[9] However, a third method, proposed by Kolar,[10] when combined with the original method of Kahn, provides a very efficient method which easily scales to higher angular momenta. Our modifications to the original method of Kahn involve the solution of the general type 2 radial integrals given by the equation (in the notation of Ref. 8)

$$Q^{N}_{\lambda\lambda'}(k_A,k_B,\alpha)=\int_0^{\infty}dr\,r^{N}e^{-\alpha r^2}M_{\lambda}(k_Ar)M_{\lambda'}(k_Br). \tag{4}$$

M_λ is a modified spherical Bessel function of the first kind, N is defined to be the sum of the powers on X, Y, and Z for both Gaussian centers, also referred to as κ, plus the power of r from the ECP projector, n_{kl} (which may range from 0 for *s*-projectors to 4 for *g*-projectors). Thus $N=\kappa+n_{kl}$. Due to symmetry, the matching angular integrals vanish unless $\kappa+\lambda+\lambda'$ is even and $|\lambda\text{-}\lambda'|\leqslant\kappa$. Also, a recursion relationship for the radial integrals may be derived directly from a standard relationship of the modified spherical Bessel functions:[11]

$$Q^{n}_{\lambda,\lambda'}=Q^{n}_{\lambda-2,\lambda'}-\frac{2\lambda-1}{k_A}Q^{n-1}_{\lambda-1,\lambda'}. \tag{5}$$

Using these relationships the number of radial integrals that must be explicitly calculated may be greatly reduced. In fact, the majority of the integrals involve $\kappa=0$, and $\lambda=\lambda'$. Thus consider:

$$Q_{\lambda\lambda}^{n_{kl}}(k_A,k_B,\alpha)=\int_0^\infty dr\, r^{n_{kl}}e^{-\alpha r^2}M_\lambda(k_A r)M_\lambda(k_B r). \tag{6}$$

The solutions to this integral are given below using the definitions presented in the Appendix to this paper (for a full derivation please refer to the supplementary material for this paper).[12] Since $n_{kl}\geqslant 0$ we need integrals for $n=(n_{kl}-2)\geqslant -2$. For $n\geqslant 0$ the following relationships can be derived:

$$B_{0,i}=\sqrt{\frac{\pi}{c}}, \tag{7a}$$

$$C_{0,i}=\sqrt{\frac{\pi}{c}}\,\mathrm{erf}(a_i\sqrt{c}), \tag{7b}$$

$$B_{1,i}=\frac{1}{c}e^{-ca_i^2}+a_i\sqrt{\frac{\pi}{c}}\,\mathrm{erf}(a_i\sqrt{c}), \tag{7c}$$

$$C_{1,i}=a_i\sqrt{\frac{\pi}{c}}; \tag{7d}$$

$$B_{n,i}=\frac{n-1}{2c}B_{n-2,i}+a_iC_{n-1,i}, \tag{8a}$$

$$C_{n,i}=\frac{n-1}{2c}C_{n-2,i}+a_iB_{n-1,i}. \tag{8b}$$

For $n<0$:

$$B_{-1,i}=2\sqrt{\pi}h(a_i\sqrt{c}), \tag{9a}$$

$$C_{-1,i}=2\sqrt{\pi}d(a_i\sqrt{c}), \tag{9b}$$

$$C_{-2,i}=4ca_ie^{-ca_i^2}+2ca_iB_{-1,i}-2cC_{0,i}, \tag{9c}$$

$$B_{-2,i}=2ca_iC_{-1,i}-2cB_{0,i}; \tag{9d}$$

$$B_{-n,i}=(1+(-1)^{n-1})\frac{(2ca_i)^{n-1}}{(n-1)(n-1)!}e^{-ca_i^2}-\frac{2c}{n-1}B_{-(n-2),i}+\frac{2ca_i}{n-1}C_{-(n-1),i}, \tag{10a}$$

$$C_{-n,i}=(1-(-1)^{n-1})\frac{(2ca_i)^{n-1}}{(n-1)(n-1)!}e^{-ca_i^2}-\frac{2c}{n-1}C_{-(n-2),i}+\frac{2ca_i}{n-1}B_{-(n-1),i}. \tag{10b}$$

Thus all of the integrals for $n<0$ are easily related to $n=-1$ and $n=0$ integrals similarly to the relationship between $n\geqslant 2$ integrals and $n=0$ and $n=1$ results. So all possible integrals can be solved in terms of relatively few basic integrals.

This method for the computation of the type 2 radial ECP integrals has been implemented into the GAMESS[13] program. This improvement along with other code modifications has resulted in a significant speedup for the ECP portion of calculations. In addition the ECP integral and derivative code has been parallelized by simply dividing up the integrals based upon shells which results in very good scalability. Table I gives some representative timings for a Ge_8C_{12} T_d geometry which will be discussed in detail later in this article. The timings illustrate the speedup over the original version due to Kahn. Specifically the speedups are about 5.5 for energies and 6.0 for gradients. In general the speedup is greater for higher angular momentum functions, thus gradients and Hessians have a higher speedup than energies. Analytic derivatives of ECPs have also been implemented through *g*-functions.

TABLE I. ECP timings (in CPU seconds on an IBM RS/6000 m370), other one and two electron integral timings included for comparison purposes.

Step	Old code	New code	New code on 2 nodes
Energy 1e-ints.	6.0	6.0	4.0
Energy ECP ints.	218.0	39.0	21.9
Gradient 1e-ints.	45.6	45.6	22.3
Gradient ECP ints.	1178.8	196.0	90.2
Gradient 2e-ints.	2523.4	2523.0	1253.8

III. CHARACTERIZATION OF THE MINIMUM ENERGY STRUCTURES OF Si_8C_{12}, Ge_8C_{12}, and Sn_8C_{12}

As interest in fullerenes and fullerene derivatives has grown in recent years, interest in the smallest fullerene like carbon cage compound, C_{20}, has also grown. Several recent studies have examined the minimum energy geometry of C_{20}.[14,15] Since many of the interesting properties of fullerenes come from the addition or substitution of metal atoms, it was of great interest when a class of stable 20-atom molecular clusters (8 metal atoms and 12 carbon atoms, referred to as metallocarbohedrenes, or metcars) were reported. In particular, Guo and co-workers have reported the formation of M_8C_{12}, where M=Ti, V, Zr, Hf, Mo, or W, through the reaction of laser vaporized titanium with a variety of hydrocarbon gases.[16] This discovery has prompted several theoretical studies attempting to predict the structures and energetics for a variety of transition metal metcars.[17] Most of these studies have considered two types of arrangements for the minimum energy structure. The first is a distorted dodecahedral structure in T_h symmetry and the second is a capped tetrahedron in T_d symmetry. Theoretical studies on Ti_8C_{12} have indicated that the T_d geometry is much more stable.[17]

Considering the similar electronic structure of main group elements such as silicon, germanium, and tin, and transition metals titanium, zirconium, and hafnium (s^2p^2 vs. s^2d^2), it is reasonable to expect similar compounds to exist. Two studies have considered Si_8C_{12},[18] however, in both of these the only geometry considered was T_h. Thus this work will examine silicon, germanium, and tin metcars, with emphasis on the minimum energy structure and lowest electronic states for each system.

IV. COMPUTATIONAL METHODS

All structures were initially optimized using the restricted Hartree–Fock (RHF) level of theory for closed shell states and the restricted open shell Hartree–Fock (ROHF) level of theory for open shell electronic states. Since many of the low-lying electronic states have many unpaired electrons in nearly degenerate orbitals, it is likely that a multiconfigurational treatment is needed. Thus, all structures were then fully reoptimized using multiconfigurational self-consistent field (MCSCF)[19] wavefunctions. The MCSCF active space used for all systems was an (8,8) active space. This active space distributes eight electrons among eight orbitals with appropriate consideration of spin and symmetry. This choice allows a full description of all open shell orbitals for all spin states through the nonet (eight unpaired electrons) spin state. The specific active spaces used contained eight nonbonding orbitals for the T_h isomer, six nonbonding plus one E–C bond/antibond pair for the D_2 isomer, and six nonbonding plus two E–C–E three-center bonding orbitals for the D_{2h} isomer.

To obtain more accurate energetics single point energies were computed using second-order perturbation theory. For the RHF and ROHF wave functions second-order Møller–Plesset perturbation theory (MP2) was used. For the MCSCF wave functions, second-order multiconfigurational quasidegenerate perturbation theory (MCQDPT2)[20] was used. In addition selected geometries were fully reoptimized using closed shell MP2 wave functions to evaluate the dependence of the geometry on the wave function type.

The basis set used was the SBKJC ECP basis set[21] on Si, Ge, Sn, and a 6-31G(d) basis set on C.[22] One set of d-type polarization functions was added to each heavy atom.[23] All structures were optimized using analytic gradients and then confirmed by computing the matrix of energy second derivatives, or Hessian, to obtain the harmonic normal modes and corresponding frequencies (each minimum has zero imaginary modes). The calculated frequencies were also used to obtain the harmonic zero-point energies used to convert energy differences to 0 K enthalpy differences.

The GAMESS[13] program was used for all calculations.

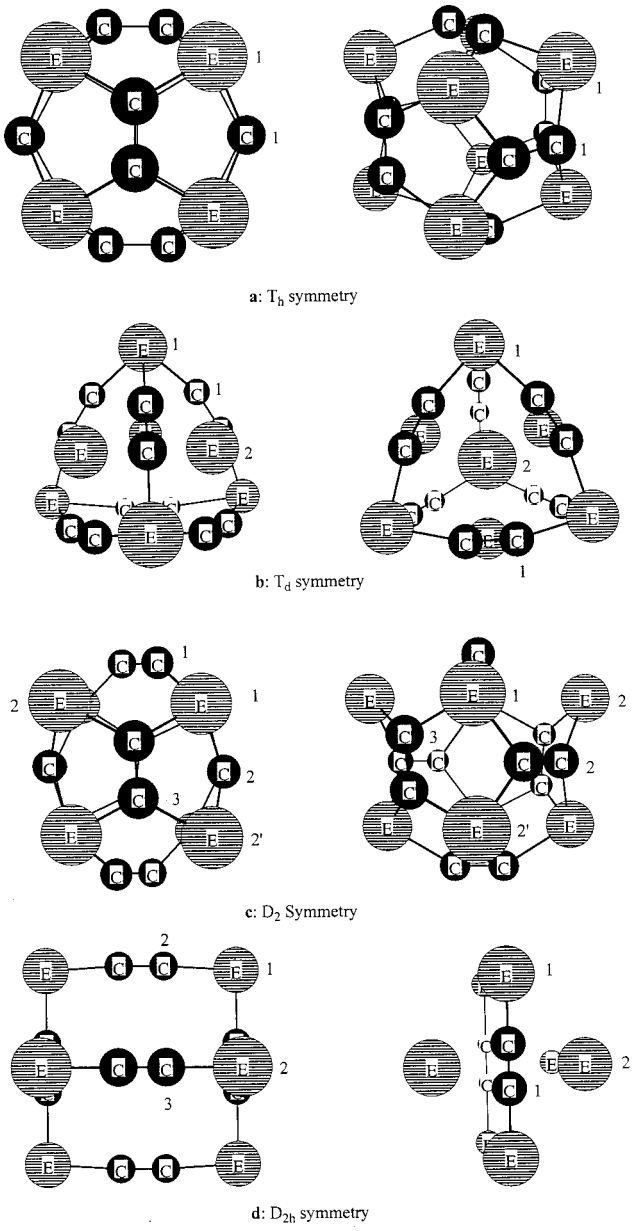

FIG. 1. Structures for E_8C_{12} (where E=Si, Ge, and Sn).

V. RESULTS

In total, four distinct geometries were considered. In addition to the expected T_h and T_d geometries, two other structures were also located, one with D_2 symmetry and one with D_{2h} symmetry. In each case, the geometry was determined only for the lowest energy spin state for that symmetry. All four geometries are illustrated in Fig. 1 with numbers indicating the symmetry unique atoms. The unique bond lengths are listed in Table II for each molecule at the RHF/ROHF, RMP2, and MCSCF levels of theory. Metal–metal interatomic distances are given for reference even though there are no metal–metal distances short enough to be considered a bond. Table III lists the relative energies of each species at the RHF/ROHF and MCSCF levels, respectively, including the RHF/ROHF zero-point energy (ZPE) correction. The corresponding spin multiplicities are also listed. The absolute energies and zero-point energy corrections as well as the complete set of Cartesian coordinates are also included as supplementary material.[12]

From Table III we conclude that although there are some significant differences in the relative energies between RHF/ROHF and MCSCF levels of theory, the qualitative energy order is the same. The same is also true of the geometries listed in Table II, which show only minor differences between the RHF/ROHF bond lengths and those optimized using MCSCF wavefunctions. For the T_h and D_2 isomers which were first optimized using high-spin ROHF wavefunctions, the MCSCF wavefunction predicts that the lowest energy state is a low-spin open shell configuration with the same number of unpaired electrons as the high-spin state. For comparison with the ROHF result, the high-spin quintet state was also optimized using an MCSCF wave function and is listed in Table III. The nonet state for the T_h geometry

TABLE II. Optimized bond lengths for Hartree–Fock (HF), RMP2, and MCSCF wavefucntions.

	Si_8C_{12}			Ge_8C_{12}			Sn_8C_{12}		
Bond	HF	MCSCF	MP2	HF	MCSCF	MP2	HF	MCSCF	MP2
T_h geometry									
E–E	3.085	3.088		3.193	3.196		3.698	3.645	3.681
E–C	1.911	1.913		1.986	1.986		2.334	2.302	2.304
C–C	1.351	1.350		1.339	1.338		1.273	1.283	1.323
T_d geometry									
E_1–E_2	3.345		3.293	3.503		3.451	3.780		3.727
E_1–C	1.967		1.944	2.075		2.054	2.269		2.253
E_2–C	2.402		2.328	2.514		2.436	2.695		2.617
C–C	1.256		1.305	1.253		1.304	1.252		1.302
D_2 geometry									
E_1–E_2	3.589	3.606		3.676	3.717		3.930	3.926	
E_1–E_2'	3.052	3.052		3.186	3.196		3.670	3.700	
E_1–C_1	1.877	1.879		1.963	1.976		2.291	2.280	
E_1–C_2	1.931	1.940		2.015	2.047		2.359	2.372	
E_1–C_3	1.892	1.879		1.969	1.975		2.304	2.294	
E_2–C_1	2.935	2.945		2.942	2.929		2.786	2.775	
E_2–C_2	1.954	1.951		2.044	2.031		2.272	2.281	
E_2–C_3	1.945	1.945		2.040	2.055		2.278	2.274	
C_1–C_1	1.215	1.214		1.217	1.218		1.231	1.231	
C_2–C_2	1.343	1.340		1.329	1.324		1.276	1.272	
C_3–C_3	1.352	1.353		1.337	1.322		1.279	1.277	
D_{2h} geometry									
E_1–E_2	3.217	3.217	3.227	3.372	3.394	3.380	3.661	3.691	3.669
E_1–C_1	1.866	1.866	1.868	1.956	1.962	1.969	2.165	2.175	2.174
E_1–C_2	1.877	1.877	1.862	1.954	1.954	1.948	2.134	2.134	2.136
E_2–C_1	2.116	2.116	2.119	2.250	2.280	2.239	2.449	2.487	2.433
E_2–C_3	1.865	1.865	1.845	1.942	1.942	1.932	2.128	2.128	2.125
C_1–C_1	1.283	1.283	1.307	1.272	1.261	1.301	1.264	1.253	1.296
C_2–C_2	1.208	1.208	1.255	1.208	1.208	1.255	1.211	1.211	1.255
C_3–C_3	1.206	1.207	1.252	1.207	1.207	1.254	1.211	1.211	1.255

using an (8,8) MCSCF wave function is identical to the ROHF reference and is therefore not repeated in the MCSCF part of the supplementary material table.

In addition to the expected T_h and T_d structures, Figs. 1(a) and 1(b), a D_2 structure, Fig. 1(c), similar to the T_h structure with two of the C_2 units twisted to a nearly linear arrangement between two E atoms, and a D_{2h} structure, Fig. 1(d), with all C_2 units arranged linearly between pairs of E atoms, were also found. Perhaps surprisingly, the D_{2h} structure is the preferred geometry at the MCSCF level of theory for the germanium and tin systems, while the T_h geometry is preferred by the silicon system. The D_2 geometry is 35–60 kcal/mol higher than the minimum energy geometry for each system. The T_d geometry is found to be quite high in energy for all three systems, and Hessians reveal that it is a high order saddle point with several normal modes which break the T_d symmetry. As the metal is changed from Si to Ge and Sn, the T_h geometry becomes much less favorable, while the D_{2h} geometry becomes more favorable.

TABLE III. SCF and MCSCF relative energies (kcal/mol).

	Si_8C_{12}		Ge_8C_{12}		Sn_8C_{12}	
Geometry	Energy	State	Energy	State	Energy	State
RHF (singlets); ROHF (triplets)						
a T_h	0.0	^9A_g	75.5	^9A_g	161.9	^1A_g
b T_d[a]	259.8	$^1A_1$	172.7	$^1A_1$	123.1	$^1A_1$
c D_2	49.4	^5A	57.7	^5A	35.9	^5A
d D_{2h}	47.1	^1A_g	0.0	^1A_g	0.0	^1A_g
MCSCF						
a T_h	0.0	^1A_g	88.5	^1A_g	165.0	^1A_g
a T_h	4.9	^9A_g	95.2	^9A_g		
b T_d[a]						
c D_2	39.6	^1A	59.9	^1A	51.6	^1A
c D_2	50.1	^5A	74.7	^5A	54.7	$^5B_2$
d D_{2h}	46.5	^1A_g	0.0	^1A_g	0.0	^1A_g

[a]Saddle point at the RHF level of theory.

Table II illustrates that as the metal is changed from Si to Ge and Sn the metal–metal (E–E) and metal–cabon (E–C) distances increase, as might be expected from the increasing atomic radius of the metal atom. Perhaps less expected is the observation that as the radius of the metal atom increases the C–C bond distance stays the same or decreases. There is also a dramatic difference in the C–C bond distance among the four isomers. In the T_h isomer the C–C bond distance of approximately 1.34 Å is characteristic of a C–C double bond. However, the C–C distance of 1.21 Å in the D_{2h} isomer indicates a C–C triple bond. Thus, there is a significant difference in the bond character between the different isomers. These compare to a C–C bond distance between 1.4–1.5 Å for C_{20} (Ref. 14) and a value of 1.4Å for the Ti_8C_{12} metcars.[18]

The D_2 and D_{2h} structures have fewer E–C bonds than the T_h structure. In the T_h structure every metal atom is directly bonded to three carbon atoms. In the D_2 structure

TABLE IV. MP2 and MCQDPT2 relative energies (kcal/mol).

	Si_8C_{12}		Ge_8C_{12}		Sn_8C_{12}	
Geometry	Energy	State	Energy	State	Energy	State
MP2//SCF						
a T_h	0.0	^9A_g	72.8	^9A_g	4.9	^1A_g
b T_d[a]	79.5	$^1A_1$	34.1	$^1A_1$	4.1	$^1A_1$
c D_2	17.0	^5A	62.1	^5A	6.8	^5A
d D_{2h}	19.7	^1A_g	0.0	^1A_g	0.0	^1A_g
MCQDPT2//MCSCF						
a T_h	0.0	^1A_g	28.4	^1A_g	−9.2	^1A_g
c D_2	45.9	^1A	9.8	^1A	−26.5	^1A
c D_2	72.3	^5A	51.6	^5A	−13.0	$^5B_2$
d D_{2h}	68.6	^1A_g	0.0	^1A_g	0.0	^1A_g
MP2//RMP2						
a T_h					3.6	^1A_g
b T_d[a]	62.6[(b)]	$^1A_1$	30.5	$^1A_1$	0.8	$^1A_1$
d D_{2h}	7.3[(b)]	^1A_g	0.0	^1A_g	0.0	^1A_g

[a]Saddle point at the RHF and MP2 levels of theory.
[b]Relative to the T_h MP2 single point energy.

the affect of twisting two of the C_2 units is to reduce the E–C bond count on four of the metal atoms. This reduction results in increased bonding for the affected C_2 units, as well as a small reduction in the bond length of the remaining E–C bonds. This effect is even greater in the D_{2h} structure, in which four of the metal atoms are directly bonded to two carbon atoms. The remaining four metal atoms are directly bonded to only one carbon atom and bridge a C_2 unit. Thus, the reduction in the number of direct metal–carbon bonds in the D_{2h} structure results in an increased bond order for the C–C bonds as well as a small increase in the bond order for the remaining metal–carbon bonds.

All of these results can probably best be described as size effects of the metal atom. As the size of the metal atom increases the length of the metal carbon bonds must also increase. In these cage structures, especially the T_h structure, this pushes the metal atoms farther from the cage center and decreases the angle between metal–carbon bonds, thus increasing the cage strain. In addition, the metal–carbon bond strength for Ge and Sn is lower than for Si due to the less effective overlap of the $4p$ and $5p$ orbital with the $2p$ of carbon. Thus, the Ge and Sn systems prefer arrangements where the carbon–carbon bond order is high at the expense of the number of metal–carbon bonds such as the D_{2h} structure.

Table IV lists the RMP2/ROMP2 and MCQDPT2 relative energies, without ZPE correction. The addition of dynamic correlation provided by perturbation theory dramatically shifts the relative energies. The primary affect is a considerable reduction in the spread of energies among the isomers. Nonetheless, the global minimum for each species is unchanged, except in the case of Sn_8C_{12}. In the latter case, the MCQDPT2 global minimum is predicted to be D_2 ^1A. To assess the effect of perturbation theory on the geometries, the isomers for which RMP2 provides an adequate description were fully reoptimized at the MP2 level of theory. The resulting energies are listed in Table IV and the optimized bond lengths are included in Table II. Since MCQDPT2 optimizations are not currently possible, further optimizations were not performed.

The MP2 optimizations do not change the relative energies dramatically, even though there is a noticeable lengthening of the C–C bonds (0.3–0.5 Å). Thus, the single point energies probably provide a good estimate of the relative ordering of the energies of each isomer. In addition, MP2 Hessians predict that the T_d isomers are high order saddle points in agreement with the RHF results. Therefore, we conclude that SCF and MCSCF wave functions seem to be adequate to get the correct basic energy order and geometries, while perturbation theory is necessary to get the correct magnitudes of the energy differences.

The vibrational frequencies with significant infrared intensities are listed in Table V. A simple description is also listed for each frequency, but since the majority of the frequencies involve the entire cluster it is necessary to view animations of each vibration to fully understand the motion of the molecule (animations are provided in the supplementary material).[12] Except for two systems where a C_2 stretch is infrared active, all of the listed frequencies involve at least four atoms, such as E–C–C–E stretches, and many involve the entire cage. Most of the low frequency vibrations involve the motion of the C_2 as a unit, either in a twisting motion about the center of the C–C bond or as a concerted motion in one direction.

VI. CONCLUSIONS

In this article we have presented an improved method for the computation of integrals involving effective core potentials. This improved method has been implemented into the GAMESS program and has been shown to significantly reduce the computational cost of ECP integrals. The improved program has been applied to the determination of the minimum energy structures of silicon, germanium, and tin analogs of the Ti_8C_{12} metcars. In addition to the two expected structures, two novel previously unreported arrangements have also been predicted.

The predicted geometries and relative energies for each isomer show that three isomers, the T_h, D_2, and D_{2h} structures, correspond to energy minima, while the fourth isomer, the T_d structure, is a high-order saddle point. The T_h structure is predicted to be the global minimum for Si_8C_{12} at all levels of theory. In contrast the D_{2h} structure is predicted to be the global minima for Ge_8C_{12}, and D_2 is predicted to be the Sn_8C_{12} global minimum at the MCQDPT2//MCSCF level of theory, which predicts the D_2 structure to be the global minima.

ACKNOWLEDGMENTS

The work described in this article was supported by grants from the Air Force Office of Scientific Research (F49-620-95-1-0073), the Department of Defense CHSSI program, and Iowa State University in the form of a Department of Education GAANN fellowship awarded to B.M.B.

TABLE V. Vibrational frequencies with an infrared intensity greater than 0.1 Debye^2/(amu Å^2).

	Si_8C_{12}		Ge_8C_{12}		Sn_8C_{12}		
Geometry	Frequency	Intensity	Frequency	Intensity	Frequency	Intensity	Type[a]
a T_h	499	1.4	484	4.3	403	3.3	cs
	499	1.4	484	4.3	403	3.3	cs
	499	1.4	484	4.3	403	3.3	cs
	568	4.1	649	0.2	567	0.4	cr
	568	4.1	649	0.2	567	0.4	cr
	568	4.1	649	0.2	567	0.4	cr
	808	3.2	690	0.8			ca
	808	3.2	690	0.8			ca
	808	3.2	690	0.8			ca
					1587	0.2	c2
					1587	0.2	c2
					2587	0.2	c2
c D_2	160	0.5	135	0.2	103	0.1	cb
	166	0.5	144	0.2			cb
	279	0.5	205	0.8	138	0.3	cb
	282	0.1	216	0.5	187	0.3	cs
	317	0.2	216	0.1	165	0.8	cb
	330	0.2			247	0.8	cs
	356	0.2			277	1.0	cr
	306	0.2			278	0.6	cs
	374	0.2	373	0.6	280	0.3	cr
	424	0.6	391	0.4	299	0.7	cs
	475	2.0	406	2.1	332	0.7	cs
	497	1.3	408	0.2			cr
	528	1.5	428	0.8	337	1.0	cr
	553	5.0	453	2.1	358	1.4	cs
			457	0.2			cs
			458	1.1	391	4.6	cs
	626	0.2	546	0.4	416	0.6	cr
	641	1.2	558	2.4	450	0.2	cr
	678	2.3	576	4.0	452	2.0	cs
	687	0.6	594	1.1			cs
			604	0.9			cr
			619	0.7			cr
	699	0.2					cs
	715	4.0	686	1.3	454	1.3	cs
	735	0.7					ca
	739	2.5	689	1.9	471	0.6	ca
	805	0.5			479	7.9	cs
	822	5.8	737	0.8	492	0.6	cs
	2295	0.1	1620	0.2			c2
d D_{2h}	262	0.1	233	0.4	188	0.8	eb
	279	0.5	239	0.4	198	0.6	eb
	307	0.7	239	0.2	195	0.3	er
			246	0.2			es
			269	0.2			es
	440	0.6	378	0.3	304	0.3	cr
	538	4.5	461	3.3	368	3.4	cr
	571	0.6	484	12.7	423	8.5	es
	606	21.3	514	0.7	441	0.6	cr
	723	0.7	600	0.2			es
	746	24.2	611	19.6	526	14.7	es
	780	32.2	654	29.0	584	30.7	es

[a]Codes: cs=symmetric cage stretch, ca=asymmetric cage stretch, cb=cage bend, cr=C_2 rocking motion, c2=C–C bond stretch, eb=E–C–C–E bend, er=E–C–C–E rock, es=E–C–C–E stretch.

APPENDIX

Included below are definitions of each term presented in the solutions to the ECP radial integral equation. Since the majority of the integrals involve $k=0$, and $l=1'$, the integral in Eq. (6) reduces to

$$Q_{\lambda\lambda}^{n_{kl}}(k_A,k_B,\alpha)=\int_0^\infty dr\, r^{n_{kl}}e^{-\alpha r^2}M_\lambda(k_Ar)M_\lambda(k_Br). \tag{A1}$$

M_λ are modified spherical Bessel functions given by

$$M_k(x)=(-1)^{k+1}\sum_{i=1}^{k}\frac{\alpha_{ik}}{x^i}\cosh(x)+(-1)^k\sum_{i=1}^{k}\frac{\beta_{ik}}{x^i}\sinh(x), \tag{A2}$$

where α and β are integer coefficients defined in Ref. 11. General Q integrals then reduce to combinations of the following:

$$\rho_n=\int_0^\infty e^{-cr^2}\sinh(k_Ar)\sinh(k_Br)r^n\,dr, \tag{A3a}$$

$$\sigma_n=\int_0^\infty e^{-cr^2}\sinh(k_Ar)\cosh(k_Br)r^n\,dr, \tag{A3b}$$

$$\overline{\sigma}_n=\int_0^\infty e^{-cr^2}\cosh(k_Ar)\sinh(k_Br)r^n\,dr, \tag{A3c}$$

$$\tau_n=\int_0^\infty e^{-cr^2}\cosh(k_Ar)\cosh(k_Br)r^n\,dr. \tag{A3d}$$

It is also convenient to make the following definitions:

$$A_n(c,a_i)=\int_{-a_i}^{\infty}e^{-cx^2}(x+a_i)^n dx, \tag{A4a}$$

$$a_1=\frac{k_A+k_B}{2c}, \tag{A4b}$$

$$a_2=\frac{|k_A-k_B|}{2c}, \tag{A4c}$$

$$\Gamma_i=\tfrac{1}{4}e^{ca_i^2}, \tag{A4d}$$

$$B_{n,i}=A_n(c,a_i)+A_n(c,-a_i), \tag{A5a}$$

$$C_{n,i}=A_n(c,a_i)-A_n(c,-a_i). \tag{A5b}$$

The above integrals then become:

$$\rho_n=\Gamma_1B_{n,1}-\Gamma_2B_{n,2}, \tag{A6a}$$

$$\tau_n=\Gamma_1B_{n,1}+\Gamma_2B_{n,2}, \tag{A6b}$$

$$\sigma_n=\Gamma_1C_{n,1}+\mathrm{sign}(k_A-k_B)\Gamma_2C_{n,2}, \tag{A6c}$$

$$\overline{\sigma}_n=\Gamma_1C_{n,1}-\mathrm{sign}(k_A-k_B)\Gamma_2C_{n,2}. \tag{A6d}$$

The solution of these integrals will involve three special functions: the error function:

$$\mathrm{erf}(x)=\frac{2}{\sqrt{\pi}}\int_0^x e^{-t^2}\,dt, \tag{A7}$$

the Dawson function:

$$\mathrm{d}(x)=e^{-x^2}\int_0^x e^{t^2}\,dt, \tag{A8}$$

and the hybrid Dawson error function:

$$\mathrm{h}(x)=e^{-x^2}\int_0^x e^{t^2}\,\mathrm{erf}(t)\,dt. \tag{A9}$$

[1] L. R. Kahn, P. Baybutt, and D. G. Truhlar, J. Chem. Phys. **65**, 3826 (1976).
[2] A. Komornicki, K. Ishida, K. Morokuma, R. Ditchfield, and M. Conrad, Chem. Phys. Lett. **45**, 595 (1977).
[3] L. R. Kahn, J. Chem. Phys. **75**, 3962 (1981).
[4] K. Kitaura, S. Obara, and K. Morokuma, Chem. Phys. Lett. **77**, 452 (1981).
[5] J. Breidung, W. Thiel, and A. Komornicki, Chem. Phys. Lett. **153**, 76 (1988).
[6] T. V. Russo, R. L. Martin, P. J. Hay, and A. K. Rappé, J. Chem. Phys. **102**, 9315 (1995).
[7] Q. Cui, D. G. Musaev, M. Svensson, and K. Morokuma, J. Phys. Chem. **100**, 10936 (1996).
[8] L. E. McMurchie and E. R. Davidson, J. Comput. Phys. **44**, 289 (1981).
[9] R. M. Pitzer and N. W. Winter, Int. J. Quantum Chem. **40**, 773 (1991).
[10] M. Kolar, Comput. Phys. Commun. **23**, 275 (1981).
[11] M. Abramowitz and I. A. Stegun, *Handbook of Mathematical Functions* (Dover, New York, 1964).
[12] See EPAPS Document No. E-JCPSA6-111-302943 for 132 files (3 MB) including the full radial ECP integral derivation and the full set of Cartesian coordinates and absolute energies with zero-point energy corrections. This document may be retrieved via the EPAPS homepage (http://www.aip.org/pubservs/epaps.html) or from ftp.aip.org in the directory /epaps/. See the EPAPS homepage for more information.
[13] M. W. Schmidt, K. K. Baldridge, J. A. Boatz, S. T. Elbert, M. S. Gordon, J. H. Jensen, S. Koseki, N. Matsunaga, K. A. Nguyen, S. Su, T. L. Windus, M. Dupuis, and J. A. Montgomery, Jr., J. Comput. Chem. **14**, 1347 (1993).
[14] Z. Wang, P. Day, and R. Pachter, Chem. Phys. Lett. **248**, 121 (1996).
[15] J. M. L. Martin, J. El-Yazal, and J. P. François, Chem. Phys. Lett. **248**, 345 (1996).
[16] (a) B. C. Guo, K. P. Kerns, and A. W. Castleman, Jr., Science **255**, 1411 (1992); (b) B. C. Guo, S. Wei, J. Purnell, S. Buzza, and A. W. Castleman, Jr., *ibid.* **256**, 515 (1992); (c) S. Wei, B. C. Guo, J. Purnell, S. Buzza, and A. W. Castleman, Jr., J. Phys. Chem. **96**, 4166 (1992); (d) B. C. Guo, K. P. Kerns, and A. W. Castleman, Jr., J. Am. Chem. Soc. **115**, 7415 (1993); (e) S. F. Cartier, Z. Y. Chen, G. J. Walder, C. R. Sleppy, and A. W. Castleman, Jr., Science **260**, 195 (1993).
[17] (a) P. J. Hay, J. Phys. Chem. **97**, 3081 (1993); (b) Z. Lin and M. B. Hall, J. Am. Chem. Soc. **115**, 11165 (1993); (c) I. Dance, *ibid.* **118**, 6309 (1996).
[18] (a) R. W. Grimes and J. D. Gale, J. Chem. Soc. Chem. Commun. **17**, 1222 (1992); (b) R. W. Grimes and J. D. Gale, J. Phys. Chem. **97**, 4616 (1993).
[19] (a) K. Ruedenberg, M. W. Schmidt, M. M. Gilbert, and S. T. Elbert, Chem. Phys. **71**, 41 (1982); (b) B. Lam, M. W. Schmidt, and K. Ruedenberg, J. Chem. Phys. **89**, 2221 (1985).
[20] H. Nakano, J. Chem. Phys. **99**, 7983 (1993).
[21] (a) For Si: W. J. Stevens, H. Basch, and M. J. Krauss, Chem. Phys. **81**, 6026 (1984). (b) For Ge, Sn: W. J. Stevens, H. Basch, and P. Jasien, Can. J. Chem. **70**, 612 (1992).
[22] (a) For H: R. Ditchfield, W. J. Hehre, and J. A. Pople, J. Chem. Phys. **54**, 724 (1971); (b) For C: W. J. Hehre, R. Ditchfield, and J. A. Pople, *ibid.* **56**, 2257 (1972); (c) The polarization exponents, $\mathrm{H}\zeta_p=1.1$ and $\mathrm{C}\zeta_d=0.8$, are given by: P. C. Hariharan and J. A. Pople, Theor. Chim. Acta **28**, 213 (1973).
[23] The exponents used were: $\mathrm{Si}\zeta_d=0.364$, $\mathrm{Ge}\zeta_d=0.254$, $\mathrm{Sn}\zeta_d=0.177$.